TECNIACUSTICA ELCHE · 2022

53º CONGRESO ESPAÑOL DE ACÚSTICA
XII CONGRESO IBÉRICO DE ACÚSTICA

TIME-HARMONIC COMPUTATION OF THE FAR-FIELD DIRECTIVITY PATTERN OF AN UNDERWATER TRANSDUCER USING NEAR-FIELD IMPULSIVE RESPONSE DATA

PACS: 43.38.−p, 43.30.+m, 43.20.Bi

Recondo Estévez, Sara
Marine Instruments. Universidade da Coruña. sara.recondo@udc.es
Prieto Aneiros, Andrés
Universidade da Coruña. CITMAga. andres.prieto@udc.es
Souto Sánchez, Martín
Marine Instruments.
Prado Cambeiro, Jaime
Marine Instruments. jprado@marineinstruments.es

Underwater acoustics, transducers, directivity pattern

ABSTRACT.

The reliability of any numerical simulation of underwater acoustic systems in marine environments requires an accurate characterization of the active transducer, which generates the acoustic field used to monitor the surrounded media. The vibrational description can be quickly done experimentally using in-house laboratory equipment where its acoustic response can be obtained from near-field impulsive measurements. However, a straightforward extrapolation of those near-field data to predict the transducer behaviour in realistic marine environments is not entirely possible since its far-field performance is not available. The present work proposes an inverse numerical methodology based on an integral representation of the pressure field. Following the classical Brekhovskikh integral methods [1], the far-field values of the acoustic pressure are determined by the so-called directivity pattern, computed by solving a regularized least-square inverse problem where the near-field data is used as the target. Since the available experimental data is limited, a low-order polynomial discretization has been utilized to discretize the directivity pattern and avoid oversampling issues. The proposed methodology has been validated in different analytical scenarios with closed-form solutions such as spherical sources and end-fire arrays. Its accuracy is illustrated by analyzing in detail the numerical quadrature techniques and the error distribution at far-field locations.

RESUMEN.

La fiabilidad de cualquier simulación numérica en el ámbito de la acústica submarina para entornos marinos requiere una caracterización precisa del transductor activo que monitoriza el medio. Su descripción vibratoria puede obtenerse inmediatamente utilizando equipo de laboratorio para medir experimentalmente su respuesta impulsiva en campo cercano. Sin embargo, no es posible extrapolar esta respuesta para predecir el comportamiento del transductor en un entorno marino real, ya que no se conoce su respuesta en campo lejano. Este trabajo propone una metodología numéric basada en una representación integral del campo de presiones. Siguiendo los métodos de integración clásicos (véase Brekhovskikh [1]), los valores del campo lejano acústico vienen determinados por el patrón de directividad, calculado mediante la resolución por mínimos cuadrados de un problema inverso basado en datos de campo cercano. Debido a que este conjunto de datos experientales es limitado, se ha utilizado una discretización basada en polinomios de bajo orden para el patrón de directividad, con el fin de evitar problemas de sobremuestreo. La metodología propuesta ha sido validada en diferentes escenarios analíticos con soluciones conocidas, como monopolos o end-fire arrays.

Su precisión se ilustra mediante el análisis de las técnicas de cuadratura empleadas y la distribución del error en campo lejano.

1. INTRODUCTION

Active acoustic transducers are widely used in very different marine applications, for fishery purposes installed in satellite buoys (see Marine Instruments products [2]), for non-destructive testing in industrial facilities [3] or for monitoring biological ecosystems [4]. In any of these cases, an accurate characterization of the input pressure field generated by the transducer is essential to determine the acoustic radiation and the vibrational response of the surrounding media, which the transducer has insonified. With the aim of predicting numerically the generated far-field at a fixed frequency, the time-harmonic near-field pressure values are assumed to be known at some specific locations (see Section 2). From this data, thanks to the solution of a least-square inverse problem, the directivity pattern will be computed (see a detailed discussion in Section 3). Finally, some numerical results are shown in Section 4.

2. GENERATED TRANSDUCER PRESSURE

Following a classical integral representation of the pressure field (see Brekhovskih [1]) the pressure field generated in a dissipative media can be computed at any spatial point once the directivity pattern $S(\theta)$ of the acoustic source (active transducer) is known as θ-dependent function, this is, depending on the angle of incidence (possible, also complex-valued). Throughout this work it is assumed that the underwater media is dissipative, this is the wave number, denoted by $k(\omega)$, is complex-valued and has a positive imaginary part. Additionally, for simplicity in the exposition, it is assumed that the generated pressure field is axis-symmetric (due to the geometrical properties of the active surface and the mounting equipment of the transducer). Hence, in what follows, the pressure field and its corresponding data will be located on the plane xz, where the half-plane with $z < 0$ is considered the underwater media and plane $z = 0$ is corresponding to the sea surface.

If the axis-symmetric directivity pattern $S(\theta)$ is known, the integral expression of an incident pressure field p_{inc} generated by an acoustic source at a point with Cartesian coordinates (x, y, z) is given by

$$p_{inc}(x,y,z) = ik(\omega)\int_0^{\pi/2-i\infty} J_0(k(\omega)r(x,y)\sin(\theta))e^{-ik(\omega)z\cos(\theta)}\,S(\theta)\sin(\theta)\,d\theta, \qquad (1)$$

where J_0 is the Bessel function of order 0, and $r(x,y) = \sqrt{x^2+y^2}$, $S(\theta)$ is the directivity function, ω is the angular frequency, and θ denotes the angle of incidence in the xz plane with respect to the origin (placed on the centre of the active surface of the transducer). The complex-valued integral path should be understood as an unbounded path in the complex plane which tends to $\pi/2 - i\infty$ on the upper part of the integral path. More precisely, in the present work an integral path composed by straight lines has been used in (1): the real-valued segment $[0, \pi/2]$ and the vertical line passing through $\pi/2$ with $\mathrm{Im}(\theta) \leq 0$. From a numerical point of view, firstly the integral expression in (1) is computed using the change of variable $u = cos(\theta)$ to avoid overflow trigonometric evaluations when the angle is complex-valued. Second, the integral value is computed using a standard composite Simpson's quadrature rule where the complex-valued path is truncated with a finite length. Such truncation preserves the accuracy of the integral value due to the exponential decay of the integrand in (1). The number of quadrature nodes is selected such that a fixed number of nodes per wavelength is guaranteed.

3. COMPUTATION OF THE DIRECTIVITY PATTERN

The directivity pattern can be approximated from the near-field values of the pressure field generated by the transducer. With this purpose, the directivity pattern $S(\theta)$ is approximated by a standard piecewise linear finite element (FE) method stated in the complex-valued path of integration involved in (1). In that manner, the discretization of $S_h(\theta)$ depends on the pointwise

values $S_h(\theta_j)$ with $0 \le j \le N$, which are the FE degrees of freedom and the FE basis functions $\phi_j(\theta)$, are given by

$$\phi_j(\theta) = \begin{cases} 1 - \dfrac{|\theta_j - \theta|}{\theta_{j+1} - \theta_j} & \text{for} \quad \theta_{j-1} \le \theta \le \theta_j \,, \\ 0 & \text{for} \quad \theta_j \le \theta \le \theta_{j+1}, \end{cases}$$

where θ_j are the vertex locations of the FE degrees of freedom in the integral complex-valued path. Consequently, the pressure field computed by using the FE discretization of the directivity pattern is given by

$$p_h(x_i, y_i, z_i) = ik(\omega) \sum_{j=0}^{N} S_h(\theta_j) \left(\int_0^{\pi/2 - i\infty} J_0(k(\omega) r(x,y) \sin(\theta)) e^{-ik(\omega) z \cos(\theta)} \phi_j(\theta) \sin(\theta)\, d\theta \right), \quad (2)$$

where (x_i, y_i, z_i) with $0 \le i \le M$ are spatial locations where the pressure field is assumed known. Notice that the number of measurement points, M, and the number of degrees of freedom used in the discretization of $S(\theta)$, N, are not equal. Obviously, (2) can be rewritten as a linear system in matrix form $A\vec{S} = \vec{b}$, where $S_j = S_h(\theta_j)$,

$$A_{ij} = ik(\omega) \int_0^{\pi/2 - i\infty} J_0(k(\omega) r(x,y) \sin(\theta)) e^{-ik(\omega) z \cos(\theta)} \phi_j(\theta) \sin(\theta)\, d\theta,$$

and $b_i = p_h(x_i, y_i, z_i)$ for $0 \le i \le M$ and $0 \le j \le N$.

Hence, given an experimental dataset $\{p_1, \dots, p_M\}$ with the known complex-valued pressure field values at the locations (x_i, y_i, z_i) with $0 \le i \le M$, the vector of FE degrees of freedom of the directivity pattern $\vec{S}$ can be computed by minimizing the least-square residual:

$$\varepsilon(\vec{R}) = \sum_{i=0}^{M} |p_i - p_h(x_i, y_i, z_i)|^2 = \sum_{i=0}^{M} \left| p_i - \left[A\vec{R} \right]_i \right|^2.$$

In this case, the computation of the directivity pattern is straightforward solving a linear system with a rectangular matrix by a least-square method.

However, in some experimental settings the data acquired from real-world measurements is phaseless and it only contains the pressure amplitude. In this case, the absence of phase information requires to reformulate the above linear least-square minimization problem into a non-linear minimization problem such that $\vec{S}(\theta) = \arg\min_{\vec{R}} \varepsilon(\vec{R})$, where

$$\varepsilon(\vec{R}) = \min_{\vec{R}} \sum_{i=0}^{M} \left(\left| \left[A\vec{R} \right]_i \right| - |p_i| \right)^2. \quad (3)$$

The non-linear least square problem stated above is also solved numerically using a classical iterative Levenberg-Marquardt algorithm [5]. An adequate estimation of the initial guess for this algorithm will be discussed in Section 4.

4. NUMERICAL RESULTS

The implementation of the generated pressure field using the integral expression (1) and the solution of the least-square inverse problems have been validated in different analytic scenarios where the exact solution is known in closed-form.

3.1. Validation tests for the generated pressure field

Attending to the definition of the directivity pattern, two different incident pressure fields with a known directivity pattern have been computed to validate the implementation of the integral expression (1). The first test corresponds to a spherical wave, namely the fundamental solution of the Helmholtz equation, which is generated by an omnidirectional acoustic source, described in terms of its directivity pattern $S(\theta) = 1$. Figure 1 shows the normalized directivity pattern (left) and the generated near-field pressure values in an underwater media around the transducer (right).

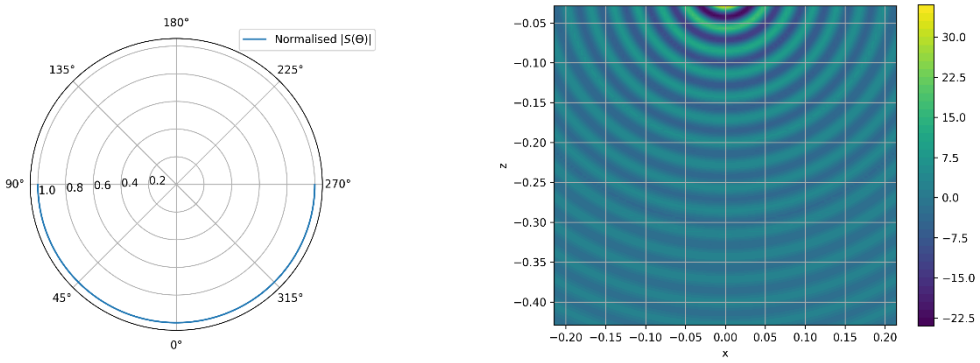

Figure 1 – Left: Directivity pattern of an omnidirectional source. Right: Real part of the incident pressure field for an omnidirectional source.

Since the numerical computation of the integral values in (1) requires the use of a quadrature rule, it has been analysed the error introduced by the composite Simpson's rule. As it is expected as soon as the number of points per wavelength (PPW) is increased, the quadrature error is decreased to reach more than four digits of accuracy (see left plot in Figure 2). Those quadrature errors are also polluting the pressure values at the near-field, but always kept the relative error lower than 3% (see right plot in Figure 2).

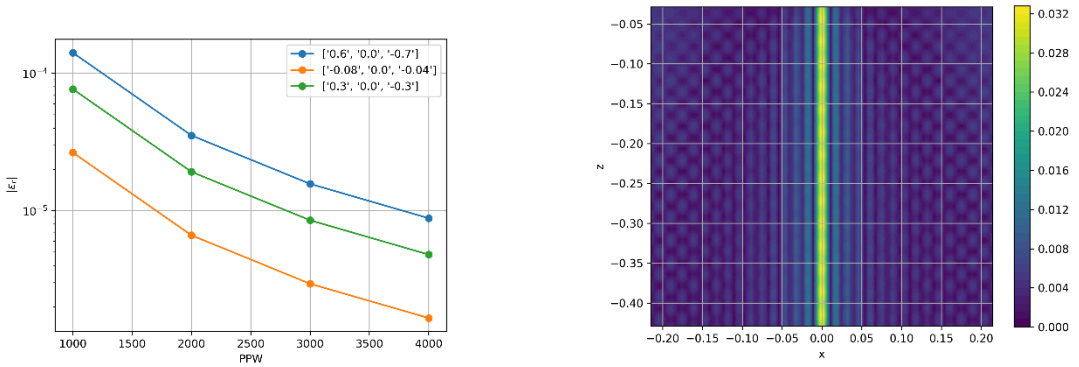

Figure 2 – Left: Relative error for the omnidirectional source in three different points plotted with respect to the number of points per wavelength. Right: spatial distribution of the relative error for the omnidirectional source.

The second test case (but without a closed-form solution for the pressure field) is given by a typical end-fire array configuration with the following directivity pattern:

$$S(\theta) = Q_0 \frac{e^{ik(\omega)L(1-\cos(\theta))}-1}{ik(\omega)(1-\cos(\theta))},$$

where Q_0 is the amplitude of the acoustic source and L is the length of the source array. The left plot in Figure 3 shows the normalized directivity pattern. The generated near-field pressure values in an underwater media around the transducer (with this end-fire array pattern) is observed in the right plot of Figure 3.

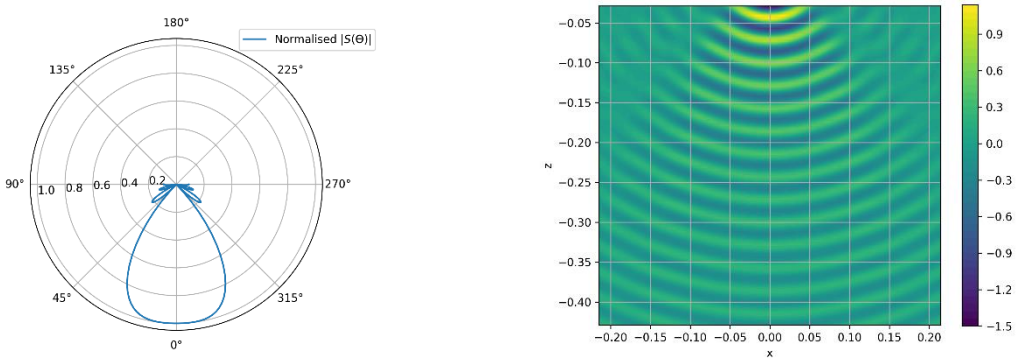

Figure 3 – Left: Directivity function of an end-fire array type source. Right: Real part of incident pressure field for an end-fire array type source.

3.2. Validation test for the computation of the directivity pattern

Now, the computation of the directivity pattern is addressed using the same scenarios described above: omnidirectional and end-fire array sources. First, the experimental dataset consists in pressure measurements with complex-valued values (amplitude and phase). The numerical results for omnidirectional source is shown in Figure 4. They have been obtained using $N = 33$, $M/N = 2$ and $N_r/N_i = 10$. The left plot in Figure 4 shows the good agreement between the approximated and exact directivity pattern. The right plot in Figure 4 shows the relative error plotted with respect to the degrees of freedom of the discretization of $S(\theta)$, where indices S_{30} to S_{33} correspond to the discretization located in the complex-path integral path used in (1).

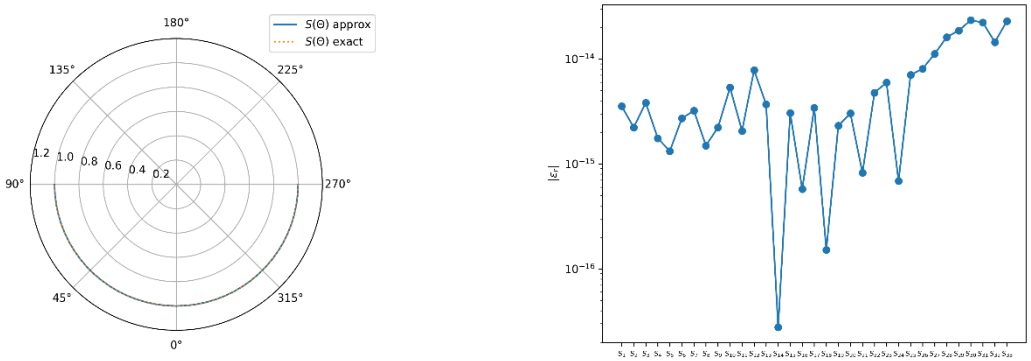

Figure 4: Left: Approximated and exact directivity pattern for the omnidirectional case. Right: Relative error plotted with respect to the FE degrees of freedom.

To analyse the accuracy of the least-square approach proposed in this work, the ratio of the number available experimental values, M, with respect to the number of discretisation points, N, has been studied. It can be observed in the left plot of Figure 5 that at least a ratio larger then 1 is required to obtain results with a high accuracy. The relation between the number of points used for the real path discretization, N_r, versus the number of points used for the imaginary path discretization, N_i, has also been studied. The right plot of Figure 5 illustrates that the variation of the number of points used in the discretization of the complex path does not seem to have a significant impact on the relative error located in the vertices of the real-valued integral path.

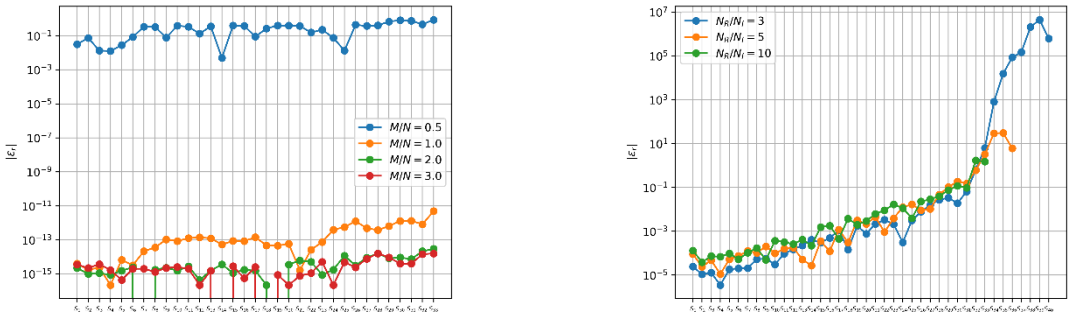

Figure 5: Left: Relative error plotted in the real-valued path for different M/N ratio in the omnidirectional test. Right: Relative error plotted in the real-valued path for different N_r/N_i ratio.

Second, an end-fire array directivity pattern has been considered. As it was shown in the omnidirectional case, the left plot of Figure 6 shows the good agreement between the approximated and the exact solution. The right plot in Figure 6 shows the relative error plotted with respect to the degrees of freedom of the discretization of $S(\theta)$, where indices S_{30} to S_{33} correspond to the discretization located in the complex-path integral path used in (1).

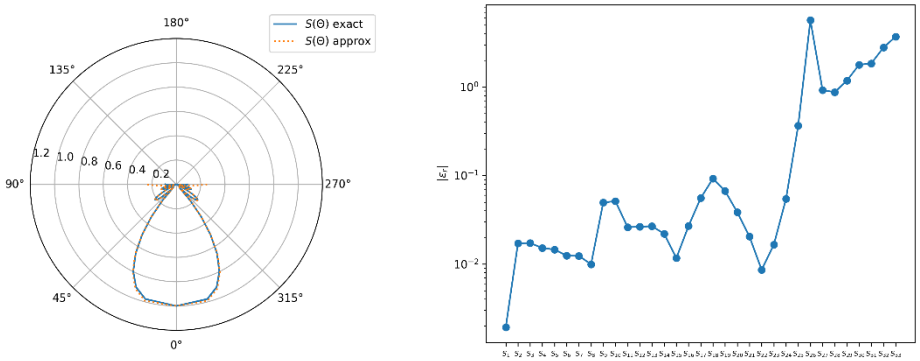

Figure 6: Left: Approximated and exact directivity pattern for the end-fire array case. Right: Relative error plotted with respect to the FE degrees of freedom.

The same discretization setting with $N = 33$, $M/N = 2$ and $N_r/N_i = 10$ has been used for the end-fire array and the omnidirectional test. Obviously, even with the same discretization, the approximated values are polluted with larger errors than the omnidirectional case due to the end-fire array has a more elaborated directivity pattern. However, despite some of the relative errors reaches values higher than 100%, the shape of the discrete directivity pattern is qualitatively analogous to the exact one.

3.2.2. Time-harmonic phaseless data

The implementation of the non-linear least-squares minimization problem has also been validated using phaseless data, this is, a dataset with only pressure amplitudes. The numerical results obtained with this non-linear approach are shown in Figures 7 and 8 for the omnidirectional and end-fire array cases, respectively.

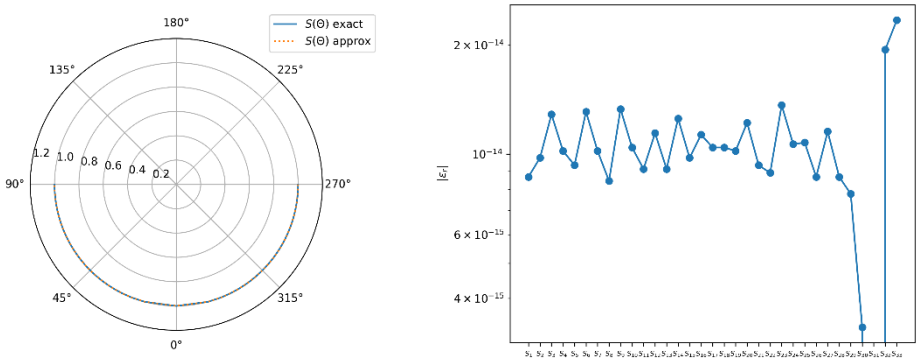

Figure 7: Left: Approximated and exact directivity pattern for the omnidirectional case. Right: Relative error plotted with respect to the FE degrees of freedom.

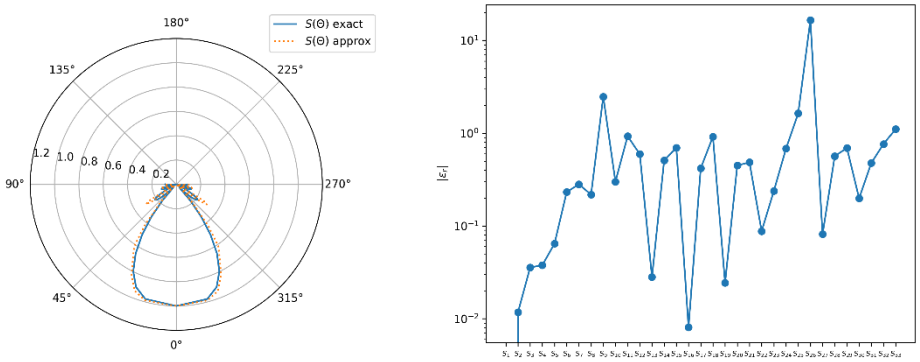

Figure 8: Left: Approximated and exact directivity pattern for the end-fire array case. Right: Relative error plotted with respect to the FE degrees of freedom.

Both Figures 7 and 8 includes the polar plot of the approximated and exact normalized directivity pattern (left plots) and the relative error plotted with respect to the FE degrees of freedom (right plots). Notice that the relative errors obtained for this non-linear problem with phaseless data have the same order of magnitude to the errors obtained for the linear least-squared problem where the dataset values included amplitude and phase.

3.3. Experimental measurements

An acoustic transducer mounted in a satellite buoy has been considered. The number of measured points used is 21 covering a total angle of 40º in the case of 50 kHz. Due to the limited number of measurement points, a spline-type interpolation has been applied in order to evaluate the near-field pressure in additional locations close to the transducer. It is important to remark that the proposed numerical approach is independent of the position of the measurement points. Here, for simplicity, the measurement points have a constant radial distance to the transducer.

Figure 9 shows the approximated directivity pattern for two different initial guesses (left plot) and the residual values at each vertex location in the integral path. The initial guesses $S_1(\theta)$ have been selected as the normalized values of the data set, while in the second case, the initial guess $S_2(\theta)$ is the solution of the linear least-square problem where the phaseless data is used as a complex-valued data with null phase.

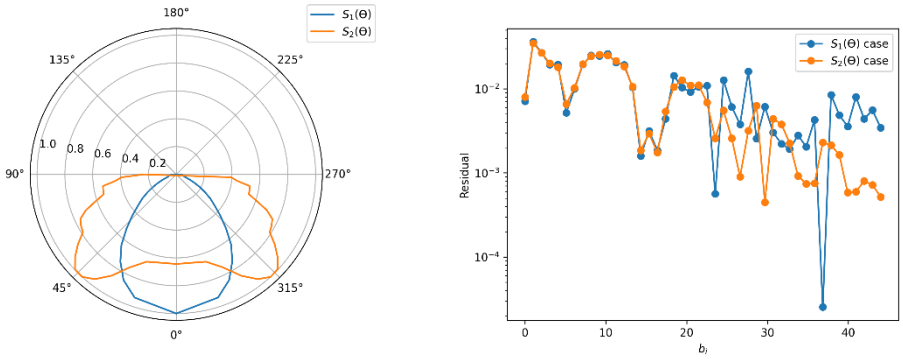

Figure 9: Left: Directivity pattern for two different initial guesses in the non-linear least-squared problem. Right: Relative residue for two different initial guesses in the phaseless problem.

4. CONCLUSIONS

The characterization of acoustic sources is usually not an easy task. This work presents a numerically methodology to characterize an acoustic source from a finite number of pressure values at known locations, regardless the distribution of the spatial measurement points and their distance to the source. Two kinds of validation test have been presented to verify the accurate results obtained from datasets where the time-harmonic pressure field is given by their amplitude and phase or only the amplitude is assumed known. The performance of the proposed approach has been illustrated in closed-form scenarios using omnidirectional and end-fire array directivity patterns but also with experimental measurements with the acoustic transducers mounted on satellite buoys provided by Marine Instruments.

REFERENCES

[1] L. Brekhovskikh. Waves in layered media. Vol. 16. Elsevier, 2012.
[2] M3i Satellite buoy. Marine Instruments, 2020. Available online in: https://www.marineinstruments.es/wp-content/uploads/2020/02/M3i-av103-EN.pdf
[3] J. Davies and P. Cawley. The application of synthetic focusing for imaging crack-like defects in pipelines using guided waves. IEEE Transactions on Ultrasonics, Ferroelectrics, Control, 56(4):759–771, 2009
[4] J. Tarrío-Saavedra, N. Sánchez-Carnero, A. Prieto. Comparative Study of FDA and Time Series Approaches for Seabed Classification from Acoustic Curves. Math Geosci 52, 669–692 (2020).
[5] J. J. More, “The Levenberg-Marquardt Algorithm: Implementation and Theory,” Numerical Analysis, ed. G. A. Watson, Lecture Notes in Mathematics 630, Springer Verlag, pp. 105-116, 1977.
[6] V.F. Humphrey and H.O. Berktay. The transmission coefficient of a panel measured with a parametric source. Journal of Sound and Vibration, 101(1):85–106, 1985